MOLECULAR AND CELLULAR BIOLOGY, Mar. 2006, p. 2309–2316 Vol. 26, No. 6
0270-7306/06/$08.00+0 doi:10.1128/MCB.26.6.2309–2316.2006

Murine Cathepsin F Deficiency Causes Neuronal Lipofuscinosis and Late-Onset Neurological Disease‡

Chi-Hui Tang,[1]† Je-Wook Lee,[1]†§ Michael G. Galvez,[1] Liliane Robillard,[1] Sara E. Mole,[2] and Harold A. Chapman[1]*

Department of Medicine and The Cardiovascular Research Institute, University of California, San Francisco, California 94143,[1] *and MRC Laboratory for Molecular Cell Biology and Department of Paediatrics and Child Health, University College London, London, United Kingdom*[2]

Received 26 August 2005/Returned for modification 19 October 2005/Accepted 21 December 2005

Cathepsin F (cat F) is a widely expressed lysosomal cysteine protease whose in vivo role is unknown. To address this issue, mice deficient in cat F were generated via homologous recombination. Although cat $F^{-/-}$ mice appeared healthy and reproduced normally, they developed progressive hind leg weakness and decline in motor coordination at 12 to 16 months of age, followed by significant weight loss and death within 6 months. cat F was found to be expressed throughout the central nervous system (CNS). cat $F^{-/-}$ neurons accumulated eosinophilic granules that had features typical of lysosomal lipofuscin by electron microscopy. Large amounts of autofluorescent lipofuscin, characteristic of the neurodegenerative disease neuronal ceroid lipofuscinosis (NCL), accumulated throughout the CNS but not in visceral organs, beginning as early as 6 weeks of age. Pronounced gliosis, an indicator of neuronal stress and neurodegeneration, was also apparent in older cat $F^{-/-}$ mice. cat F is the only cysteine cathepsin whose inactivation alone causes a lysosomal storage defect and progressive neurological features in mice. The late onset suggests that this gene may be a candidate for adult-onset NCL.

The human genome contains 11 papain-family cysteine proteases, several of which have restricted tissue expression and specific, nonredundant functions (3, 37). Cathepsin F (cat F), known to have widespread tissue mRNA expression, is a relatively understudied member of this enzyme family. cat F is unique among papain-type cathepsins due to an elongated N-terminal pro-region, which contains a cystatin-like domain attached with a flexible linker to the canonical papain-type catalytic domain (31). The enzyme contains a typical signal peptide and is found within the endosomal compartment of cells (41). Several prior studies have demonstrated in vitro that cat F is a potent endoprotease. Recombinant active cat F degrades the major histocompatibility complex (MHC) class II chaperone, invariant chain (Ii), as well or better than cathepsin S (cat S) (33). More recently, cat F has been implicated in lipoprotein biology by virtue of its ability to inhibit cholesterol efflux from peritoneal macrophages in vitro (17) and to degrade apolipoprotein B100 in vitro (26). However, a physiological role for cat F has not been established.

Numerous enzyme deficiencies are accompanied by accumulation of undegraded substrates within lysosomes, resulting in lysosomal storage diseases. Among these are mucopolysaccharidoses, glycoproteinoses, sphingolipidoses, and lipidoses (reviewed in reference 40). The neuronal ceroid lipofuscinoses (NCLs) are a collection of diseases involving lysosomal storage manifested by gross accumulation of autofluorescent lipofuscin-like material. The features of NCL include progressive loss of motor skills and vision, mental decline, myoclonus, seizures, and premature death (23). Notably, the pathological manifestations of NCL are mostly localized to the central nervous system (CNS) without visceral involvement (22). The identified gene defects linked to NCL characteristically exhibit autosomal-recessive transmission, and most encode proteins that localize to the endosomal/lysosomal compartment. Several of these are lysosomal enzymes, including palmitoyl protein thioesterase 1 (PPT1) and tripeptidyl peptidase 1 (TPP1) (25, 29). Deficiency in cathepsin D (cat D), an aspartyl endoprotease, also results in an NCL-like phenotype, along with more widespread visceral lysosomal abnormalities (16), as does the engineered mouse model lacking PPT2 activity (11). However, the identified causes of NCL are largely responsible for disease beginning in infancy or childhood. There is a paucity of genetic information or etiological mechanism available for adult-onset NCL, also referred to as Kufs disease (1, 8). Of the reported murine or human single cysteine cathepsin deficiencies, none have been associated with neuronal lysosomal defects.

A cat F-deficient mouse was generated by homologous recombination. cat $F^{-/-}$ mice developed a progressive neuropathological process that ultimately proved fatal. The present study examines the underlying cellular and molecular basis for these manifestations in cat $F^{-/-}$ mice and its possible relation to late-onset human NCLs.

MATERIALS AND METHODS

Generation of mice with targeted disruption of cat F. Exon 7 (which contains the active-site cysteine critical for enzyme activity), exon 8, and exon 9 of the murine cat F gene were deleted by homologous recombination with a targeting

* Corresponding author. Mailing address: University of California, San Francisco, Box 0111, San Francisco, CA 94143. Phone: (415) 514-0896. Fax: (415) 502-4995. E-mail: hal.chapman@ucsf.edu.

† C.-H.T. and J.-W.L. contributed equally to this study.

‡ Supplemental material for this article may be found at http://mcb.asm.org/.

§ Present address: Dana-Farber Cancer Institute, D1440, 44 Binney St., Boston, MA 02115.

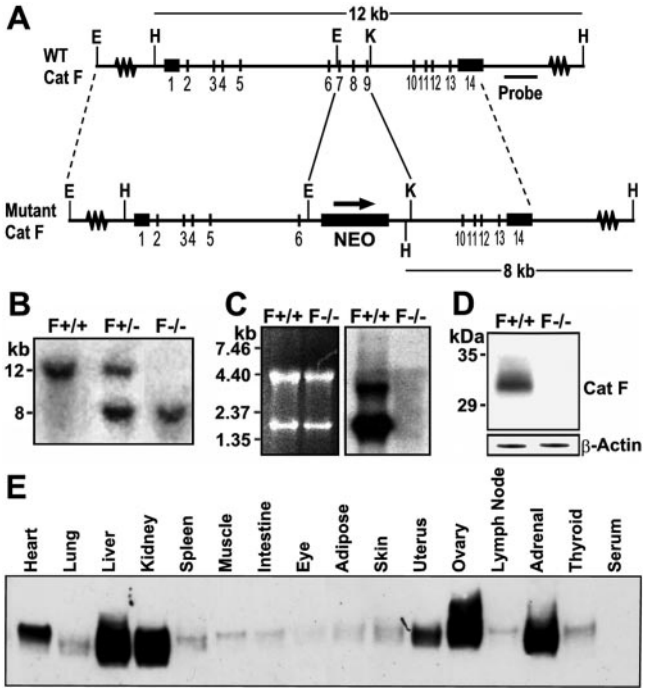

FIG. 1. Targeted disruption of the cat F gene. (A) Scheme for the targeted disruption of murine cat F gene by homologous recombination. Exons are indicated by number. E, EcoRI; H, HindIII; K, KpnI. (B) Southern blot analysis of HindIII-digested ES genomic DNA using an external probe denoted in panel A. Expected fragment sizes are 12 kb for WT and 8 kb for mutant cat F. (C) Northern blot analysis of cat F expression. The right panel shows that the expected 3.5- and 1.8-kp products are apparent in cat $F^{+/+}$ but not cat $F^{-/-}$ RNA. In the left panel, rRNA was used as a control. (D) Immunoblot analysis of cat F expression (31 kDa) in cat $L^{-/-}$ and cat L/cat F double-null liver extracts. (E) cat F immunoblot analysis of visceral tissues from a cat $L^{-/-}$ mouse. Equal protein amounts were used for each sample.

vector containing a neomycin (*neo*) cassette between the EcoRI and KpnI restriction sites in the cat F gene (Fig. 1A). G418-resistant clones were screened by Southern blot analysis of embryonic stem (ES) cell genomic DNA, which was digested with HindIII and hybridized with an external probe. Mutated ES cells were microinjected into blastocysts of 129 SVJ females at Xenogen (Cranbury, NJ). The resulting chimeras were used to generate heterozygous and subsequently homozygous mutant offspring against C57BL/6J genetic background. Mice were genotyped for the introduced cat F gene mutation by analysis of tail genomic DNA using exon 7- and *neo*-specific PCR primers (cat F-5′ [5′-ACA GAACTTGTGCTGCTCAGG-3′] and cat F-3′ [5′-TTCCTACTTCTGGGA CTCCAACC-3′] for wild type [WT] [247 bp] and cat F-5′ and Neo-3′ [5′-TGG ATGTGGAATGTGTGCGAG-3′] for knockout [225 bp]). Disruption of the cat F gene was confirmed by Northern and Western blot analyses.

The mice used in the present study are of mixed background (C57BL/6J and 129 SVJ), and littermate controls were used for all experiments. All experiments involving animal use were approved by the Institutional Animal Care and Use Committee of the University of California, San Francisco.

Immunoblotting. A rabbit polyclonal cat F antibody was generated for analysis of cat F protein expression using recombinant human cat F (kindly provided by Amos Baruch, Celera Diagnostics). Because the cat F antibody exhibited cross-reactivity with cathepsin L (cat L), immunoblots for cat F were performed with cat $L^{-/-}$ tissues. In addition, tissues from cat L/F double-null mice were used as negative controls (not shown). Tissues were lysed in a buffer containing 50 mM Tris-HCl (pH 7.4), 150 mM NaCl, 1 mM EDTA, 1% Triton X-100, 0.1% sodium dodecyl sulfate (SDS), 1% sodium deoxycholate, 0.1 mg of Pefabloc/ml, and Protease Inhibitor Cocktail (Sigma) at 1:1,000. Lysate protein concentrations were determined with the Micro BCA Protein Assay Kit (Pierce). Then, 25 to 50 μg of lysate was fractionated by SDS-polyacrylamide gel electrophoresis (PAGE) and analyzed by immunoblotting as described previously (35). Mitochondrial ATP synthase subunit c accumulation was detected by using a purified rabbit antibody (a generous gift from J. Ezaki, Juntendo University, Tokyo, Japan). The spinal cord was minced and homogenized by sonication in Tris-HCl (pH 7.4) with 1% Triton X-100 and protease inhibitors. The protein concentration was determined, and 5 μg of homogenate was solubilized by sonication in LDS sample running buffer (Invitrogen), fractionated, and analyzed by immunoblotting.

Footprint pattern test. The footprint patterns of mice were evaluated at 6, 12, and 16 months essentially as described previously (13). A distinct nontoxic paint color was used for each paw to facilitate footprint pattern analysis. Each mouse was tested at least twice.

Grid walk analysis for motor coordination. The grid walk, originally a test for motor coordination in rats, has more recently been adapted for use in mice (32). Mice were trained to transverse the grid walk apparatus prior to actual test runs. Runs were videotaped, and genotype information was blinded during analysis and scoring.

Cysteine protease active site labeling. Tissues were lysed in a solution containing 50 mM sodium acetate (pH 5.5), 1 mM EDTA, 0.1% CHAPS {3-[(3-cholamidopropyl)-dimethylammonio]-1-propanesulfonate}, 0.5% NP-40, 0.1 mg of Pefabloc/ml, and 5 μg of pepstatin A/ml (RIPA buffer) for 1 h at 4°C. Equal amounts of lysate from each tissue were labeled with ^{125}I-JPM565 (20, 28) for 1 h at 37°C and then diluted in SDS sample buffer and boiled for 10 min. Samples were fractionated by SDS-PAGE (12.5% gel), dried, and visualized by autoradiography.

For active-site labeling of cat F, single-cell suspensions were generated essentially as described previously (19). Briefly, regions of the CNS were surgically separated and minced in Hanks balanced salt solution supplemented with 10 mM HEPES and 33.3 mM glucose. The tissues were then incubated with trypsin (0.05%) and DNase I (100 U/ml) for 15 to 25 min at 37°C and gently triturated by using a fire-polished glass pipette. Single-cell suspensions were obtained by passing the resulting slurry through a 40-μm-pore-size mesh. For labeling, the cell suspension was incubated with ^{125}I-JPM565 (ethyl ester) for 1 h at 37°C, washed three times, and lysed with RIPA buffer. cat F was immunoprecipitated by using an anti-cat F antibody, pelleted with protein-A agarose beads, eluted with sample running buffer, and fractionated by SDS-PAGE. The gel was subsequently dried and visualized by autoradiography.

Light microscopy. Mice were sacrificed by isofluorane overdose, exsanguinated, and perfused with phosphate-buffered saline (PBS). Animals were subsequently perfusion fixed with 4% paraformaldehyde (PFA), and appropriate tissues were extracted. Spinal cord sections (50 μm) were cut and stained with cresyl violet or hematoxylin and eosin (H&E) for light microscopy.

Fluorescence microscopy. OCT (Sakura Finetek, Torrance, CA) embedded sections (5 to 10 μm) were mounted directly onto gelatinized slides and dried. For autofluorescence, sections were rinsed to remove OCT, dried, and mounted without staining. For immunofluorescent staining, acetone-methanol-fixed slides were permeabilized with PBS plus 0.5% Triton X-100 and blocked with 1% bovine serum albumin and 5% goat serum in PBS, followed by an overnight incubation with rabbit anti-cat F antibody and rat anti-Lamp-2 antibody (BD Pharmingen, San Diego, CA) at 4°C. After three washes with PBS, sections were incubated with secondary antibodies for 1 h and washed three times with PBS. Nuclei were stained with DAPI prior to mounting. Glial fibrillary acidic protein (GFAP) staining was carried out on PFA-fixed sections with a rabbit anti-GFAP antibody (Zymed Laboratories, South San Francisco, CA).

Electron microscopy. Mice were perfusion fixed with a solution of 2% PFA, 2% glutaraldehyde, and 4% sucrose in 0.1 M phosphate buffer (pH 7.4). The brain and spinal cord were subsequently extracted and fixed in the same solution for an additional 5 h. The tissue was treated with 1% osmium tetroxide for 4 h, dehydrated, and embedded in Epon for sectioning. Thin sections (90 nm) were stained with lead citrate for electron microscopy (14).

Clinical details of late-onset NCL patients. Thirteen patients with NCL that had not been defined genetically were included in the study. The age of onset ranged between teenage and mid adulthood, with most having no visual problems.

RESULTS

Characterization of cat F-null mice. Several correctly targeted ES cell clones were isolated and injected into blastocysts, two of which developed germ line transmission. The analysis of only one line is presented in the manuscript because the two lines proved to be indistinguishable. Southern blot analysis of tail genomic DNA revealed the expected mutant band size (Fig. 1B). Subsequent Northern blotting of liver mRNA

showed the loss of detectable cat F mRNA in homozygous mutant mice (Fig. 1C), and immunoblotting demonstrated the complete loss of detectable cat F protein in homozygous mutant mice (Fig. 1D), confirming successful targeting of cat F. cat $F^{-/-}$ mice were viable at birth, developed normally, and exhibited physical, behavioral, and reproductive characteristics indistinguishable from those of WT and heterozygous littermate controls.

Using an affinity-purified cat F antibody, we determined the pattern of cat F tissue expression in cat $L^{-/-}$ mice (Fig. 1E). cat F was found to be highly expressed in the adrenal gland, liver, kidney, testis (not shown), and ovary and moderately expressed in the heart and uterus. Lower levels of cat F protein were observed in the remaining tissues tested. These findings are consistent with prior reports of cat F mRNA distribution (4, 41). Depending on the tissue, cat F appears as two to four bands between 30 and 34 kDa, representing distinct glycosylation variants (unpublished data). H&E staining of these tissues revealed no morphological abnormalities at any age examined up to 16 months.

Because of prior reports that cat F can mediate degradation of MHC class II-associated invariant chain (33), we examined MHC class II maturation in splenocytes and bone-marrow derived and peritoneal macrophages from cat $F^{-/-}$ mice and from cat F/S double-null mice, obtained by cross-breeding cat $S^{-/-}$ and cat $F^{-/-}$ mice. However, no defects in Ii processing attributable to cat F could be discerned in any of these mice (see the supplemental material).

cat F-deficient mice develop age-related neuromuscular abnormalities. cat $F^{-/-}$ mice at approximately 1 year of age were noticed to have difficulty walking. Further examination revealed hind leg weakness, decline in motor coordination, and general wasting (Fig. 2A). Onset of observable phenotype in cat $F^{-/-}$ mice is between 12 to 16 months. Every cat $F^{-/-}$ mouse allowed to reach 16 months of age invariably developed severe symptoms ($n > 20$).

Footprint pattern analysis was performed to assess differences in gait characteristics between WT and cat $F^{-/-}$ mice. Gait patterns of 12-month-old mice did not appear to differ between WT and cat $F^{-/-}$ mice. It was noticed that cat $F^{-/-}$ mice tended to have decreased stride length relative to controls. At 15 months of age, clear irregularities in the gait of cat $F^{-/-}$ mice were observed compared to age-matched control mice (Fig. 2B). In order to assess motor coordination quantitatively, age-matched WT and cat $F^{-/-}$ mice were subjected to the grid walk test. Motor coordination in 8-month-old mice was indistinguishable between the two groups. However, 12-month-old cat $F^{-/-}$ mice exhibited a significant loss in motor coordination of the hind limbs over time and compared to age-matched WT mice (Fig. 2C).

Tonic hind leg extension, poor balance, tremors, and spastic movement were commonly observed in symptomatic cat $F^{-/-}$ mice. Two cases of spontaneous seizures have also been observed in cat $F^{-/-}$ mice with severe symptoms. An examination of the clasping response during tail suspension demonstrated a prominent tonic hind leg extension in cat $F^{-/-}$ mice rather than the expected clasping of the hind legs toward the midline, as has been reported in NCL and CNS legions (10). cat $F^{-/-}$ mice suspended by the tail maintained tonic extension and failed to grasp objects with the hind legs, which in WT mice is

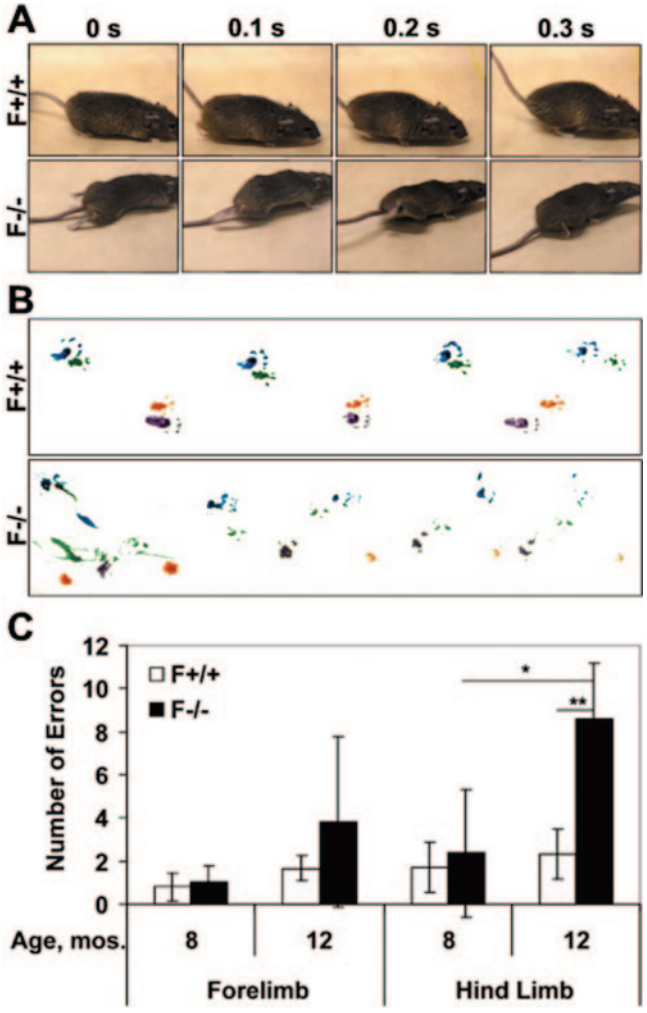

FIG. 2. Hind leg weakness and irregularities in gaits of cat $F^{-/-}$ mice. (A) Frame-by-frame video analysis of strides taken by 15-month-old cat $F^{+/+}$ and cat $F^{-/-}$ mice. (B) Footprint pattern analysis of 15-month-old cat $F^{+/+}$ and cat $F^{-/-}$ mice. Green, left forelimb; red, right forelimb; blue, left hind limb; purple, right hind limb. (C) Grid walk analysis of age-matched cat $F^{+/+}$ and cat $F^{-/-}$ mice. Student *t* test results were determined. **, 12-month-old cat $F^{+/+}$ versus cat $F^{-/-}$ mice ($P < 0.009$); *, 8-month-old versus 12-month-old cat $F^{-/-}$ mice ($P < 0.04$), 8-month-old cat $F^{+/+}$ mice ($n = 3$), 8-month-old cat $F^{-/-}$ mice ($n = 4$), 12-month-old cat $F^{+/+}$ mice ($n = 3$), and 12-month-old cat $F^{-/-}$ mice ($n = 5$).

a vigorous reflex. When allowed to age after onset of symptoms ($n = 8$), all cat $F^{-/-}$ mice exhibited progressive worsening of phenotype and died within 4 to 6 months, whereas littermate controls remained healthy.

Body weights of WT and cat $F^{-/-}$ mice did not differ prior to the onset of symptoms. Weight loss concomitant with the development of neuropathologic symptoms in cat $F^{-/-}$ was evaluated. Tracking of body weights of mice between 9 and 13 months of age revealed that WT mice gained an average of 0.4 g per month, whereas cat $F^{-/-}$ mice lost on average 0.8 g per month (not shown). A significant difference in weight change between the two groups was reached at 12 months of age.

cat F in the CNS. To explore the basis for the observed neurological features, cat F expression in the CNS was exam-

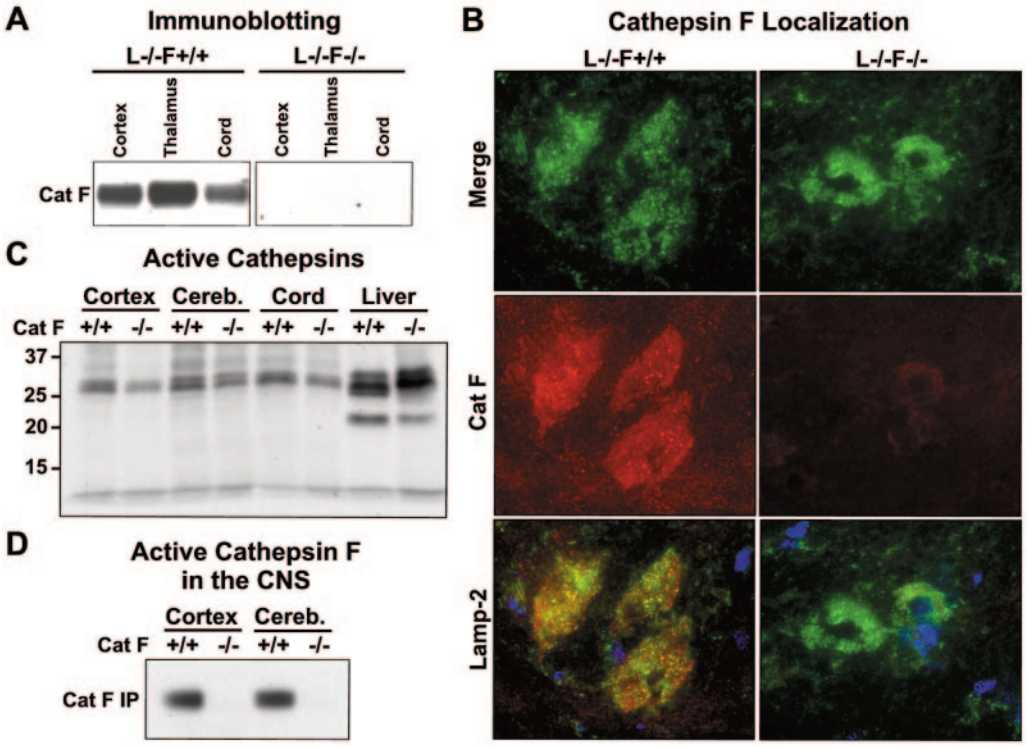

FIG. 3. Characterization of cat F in the CNS. (A) cat F immunoblot analysis of regions of the CNS from cat $L^{-/-}$ and cat L/cat F double-null mice. (B) Subcellular localization of cat F. Spinal cord sections were double stained for cat F (red) and Lamp-2 (green). The nuclei were stained with DAPI (blue). Colocalization of cat F and Lamp-2 in lysosomes is represented in yellow. (C) JPM labeling of active cysteine cathepsins. Cortex, cerebellum, spinal cord, and liver lysates from 3-month-old cat $F^{+/+}$ and cat $F^{-/-}$ mice were radiolabeled with ^{125}I-JPM565 and fractionated by SDS-PAGE. Equal amounts of protein were used for each sample. (D) JPM labeling of single-cell suspension from cortex and cerebellum of WT and cat $F^{-/-}$ mice. Intact cells were labeled with ^{125}I-JPM565 and lysed. cat F was immunoprecipitated with anti-cat F antibody, fractionated by SDS-PAGE, and visualized by autoradiography.

ined. Analysis of cat F expression by immunoblotting revealed expression throughout the CNS (Fig. 3A and data not shown). Lysosomal localization of cat F had been previously suggested (31, 41). To confirm this conclusion in the CNS, brain and spinal cord sections were simultaneously stained with cat F and Lamp-2 antibodies. cat F was shown to have a granular distribution and colocalized mostly with Lamp-2, indicating lysosomal localization (Fig. 3B). The lack of cat F staining in cat L/cat F double-null spinal cord and brain sections demonstrated specificity of the antibody for cat F and confirmed the absence of cat F expression.

Cathepsin activity in vivo. To assess the activity of cathepsins in vivo, cortex, cerebellum, lumbar spinal cord, and liver tissue lysates from 3-month-old mice were radiolabeled with ^{125}I-JPM565, an irreversible inhibitor of all active papain-type cathepsins, and fractionated by SDS-PAGE (Fig. 3C). No differences in cysteine cathepsin activity were observed between WT and cat $F^{-/-}$ mice. Remarkably, however, CNS extracts contained few active cathepsins compared to the liver, in which multiple active cathepsins were seen. The scope of active cathepsins expressed in the kidney or purified inflammatory macrophages were similar to that observed in the liver (not shown). The lack of demonstrable cat F activity in tissue lysates indicates that either cat F is unstable in tissue lysates or the amounts of active enzyme in vivo must be low. To explore this issue further, single-cell suspensions of cortex, cerebellum, and spinal cord from WT and cat $F^{-/-}$ mice were labeled with ^{125}I-JPM565, and then cat F was immunoprecipitated and analyzed by SDS-PAGE. Immunoprecipitation of cat $F^{+/+}$ cortical and cerebellar cells revealed a single 31-kDa band consistent with the size of active cat F (Fig. 3D). The complete absence of this band in cat $F^{-/-}$ cells confirmed the activity to be that of cat F. cat F activity was not evident in labeled WT spinal cord cells by this technique, probably due to the lower protein content of the lysates available for immunoprecipitation and the difficulty of generating a single-cell suspension of the spinal cord.

Histological signs of neuronal abnormality and stress. Histological examination of the lumbar spinal cord and sciatic nerve of symptomatic cat $F^{-/-}$ and age-matched control mice was carried out to assess differences in neural morphology. Staining of Nissl substance by cresyl violet in lumbar spinal cord sections revealed no obvious disparity in neurons of cat $F^{-/-}$ mice (Fig. 4A). Immunohistochemical staining for the glial cell marker GFAP in brain and spinal cord sections revealed substantial gliosis in cat $F^{-/-}$ mice compared to age-matched WT controls (Fig. 4B), which indicates neuronal stress or neurodegeneration (9) and which occurs in NCL patients and mouse models (21, 38). Quantification of GFAP staining in four matched regions of the cortex and spinal cord demonstrated an average of ~6.7-fold increase in gliosis in cat

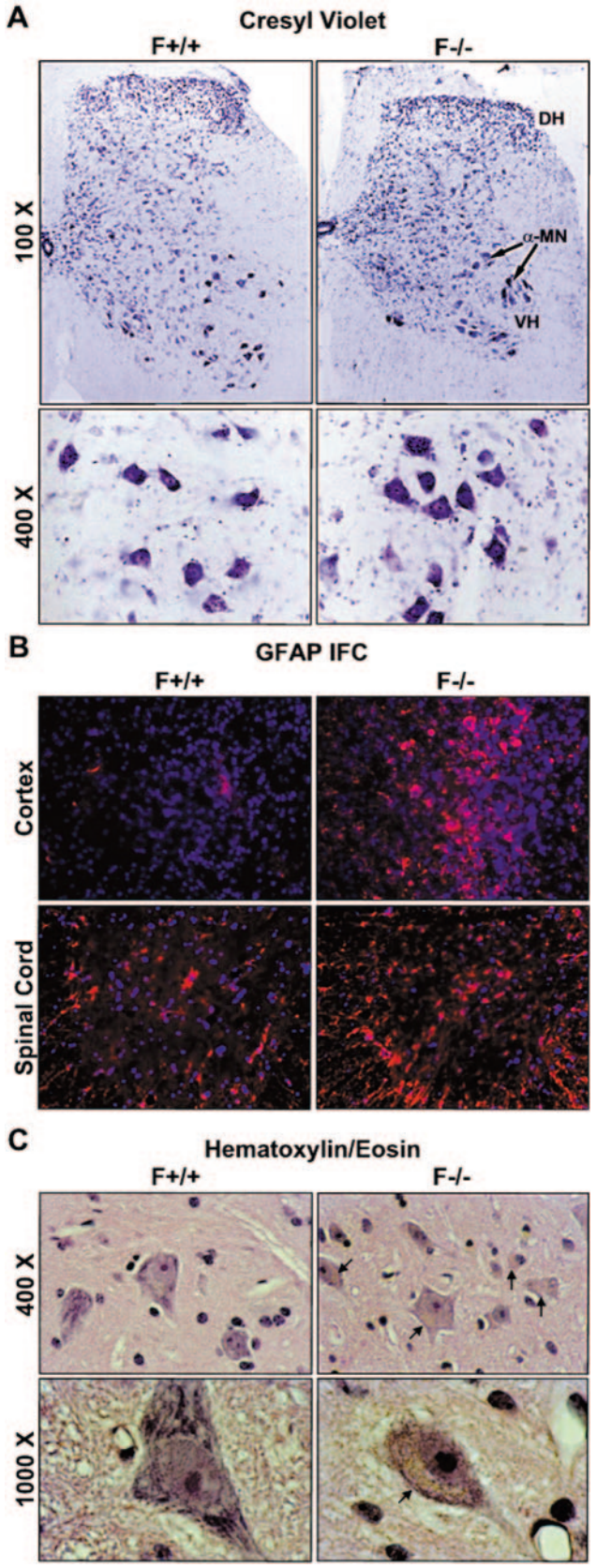

FIG. 4. Histologic analysis of mouse CNS sections. (A) Cresyl violet staining of old cat $F^{+/+}$ and cat $F^{-/-}$ lumbar spinal cord. DH, dorsal horn; VH, ventral horn; α-MN, alpha-motorneuron. (B) GFAP immunofluorescence staining (red) of the cortex and the ventral horn region of the spinal cord from 15-month-old cat $L^{-/-}$ and cat L/cat F double-null mice at ×200 magnification. Nuclei were stained with DAPI (blue). (C) H&E staining of the ventral horn region of the lumber cord from old cat $F^{+/+}$ and cat $F^{-/-}$ mice. Arrows indicate the accumulation of eosinophilic granules in the cytoplasms of neurons and glial cells.

$F^{-/-}$ mice. In addition, the measurement of brain weights in a cohort of four WT and six cat $F^{-/-}$ mice older than 7 months revealed a significant decrease in the brain masses of cat $F^{-/-}$ mice ($P = 0.035$), which suggests neuronal loss in cat $F^{-/-}$ mice. H&E staining of symptomatic cat $F^{-/-}$ lumbar cord sections demonstrated a striking accumulation of cytoplasmic eosinophilic granules in most neurons and some glial cells (Fig. 4C). A yellowish brown hue was appreciated in the granules. Age-matched WT spinal cord sections showed no obvious accretion of eosinophilic material. Staining of the sciatic nerves did not reveal any morphological changes in cat $F^{-/-}$ mice (not shown).

Accumulation of autofluorescent granules in the CNS of cat F knockout mice. The examination of unstained spinal cords of 12-month-old cat $F^{-/-}$ mice by using fluorescence microscopy revealed abundant accumulation of broad-spectrum autofluorescence within neurons and glial cells (Fig. 5A). Age-matched spinal cords from WT mice showed sparse autofluorescence, which is expected since autofluorescent pigments are known to accumulate with age (2). The amount of autofluorescent pigments in spinal cords from 3-month-old cat $F^{-/-}$ mice exceeded that of 12-month-old WT mice (not shown), indicating a substantially accelerated rate of accumulation with age in the absence of cat F. Analysis of spinal cord sections under high magnification demonstrated a striking increase of autofluorescent cytoplasmic granules in cat $F^{-/-}$ cords (Fig. 5A).

Analysis of brain sections from cat $F^{-/-}$ mice demonstrated an abundance of autofluorescent neurons throughout the brain, including notably the cerebral cortex, hypothalamus, and cerebellum (Fig. 5B). Purkinje cells of the cerebellum, which express moderate levels of cat F in cat $F^{+/+}$ mice, showed substantial autofluorescence in cat $F^{-/-}$ mice without obvious loss of Purkinje cells. Brain sections from age-matched WT mice contained few autofluorescent cells. Examination of visceral tissues revealed an absence of autofluorescent granules in both WT and cat $F^{-/-}$ mice (not shown).

Ultrastructural examination of motor neurons from the lower spinal cord. Accumulation of yellowish brown cytoplasmic granules that exhibit broad-spectrum autofluorescence was strongly suggestive of lipofuscin. To confirm the presence of accumulated autofluorescent lipofuscin-like globules, spinal cord sections of cat $F^{-/-}$ mice were analyzed by electron microscopy (EM). Ultrastructural assessment of spinal cord motorneurons revealed substantial accumulation of membrane-bound lamellar inclusions, which is consistent with lipofuscin (Fig. 6A). The granules were characterized by mostly mixed fingerprint and lamellar profiles and varied in size and shape. Prominent within many of the lipofuscin containing lysosomes was the presence of a lipid droplet. An examination of CNS mitochondria did not reveal overt ultrastructural abnormalities in cat $F^{-/-}$ mice.

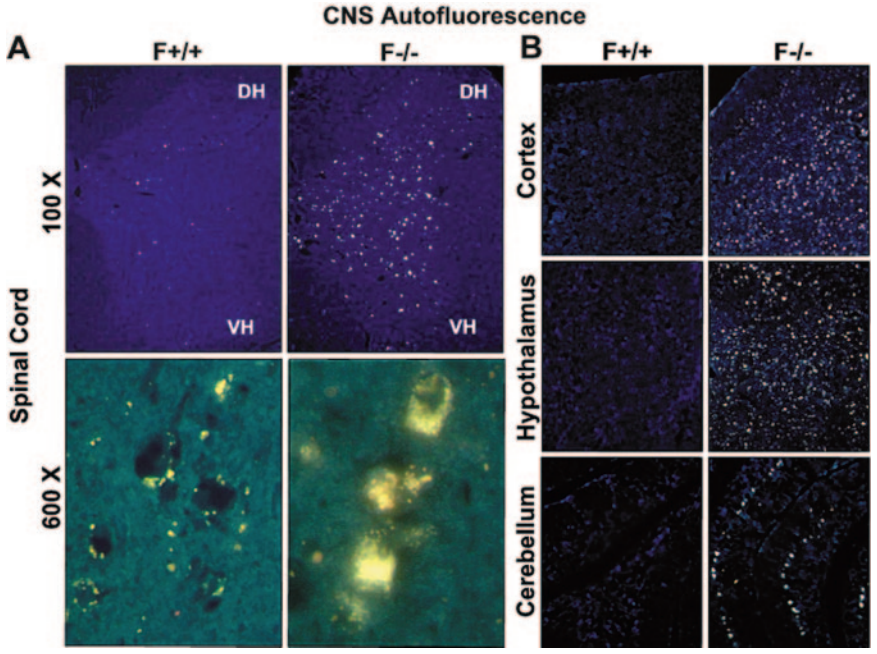

FIG. 5. Increased autofluorescence in spinal cord sections from old cat $F^{-/-}$ mice. (A) Composite image of blue, red, and green fluorescence emissions of unstained spinal cord sections at ×100 and ×600 magnifications. White light represents fluorescence emission at all three wavelengths. DH, dorsal horn; VH, ventral horn. (B) Autofluorescence in regions of the brain from 16-month-old mice.

A major constituent of lamellar-like inclusions in NCL is mitochondrial ATP synthase subunit c (6). Immunoblotting was performed to determine whether the accumulated lipofuscin granules in cat F-deficient mice contain subunit c. However, no difference in subunit c protein amounts was observed between lysates of 19-month-old cat F WT and cat $F^{-/-}$ spinal cords prepared by methods previously shown to extract subunit c from lipofuscin (6) (Fig. 6B). Total subunit c levels were also not different between 3- and 19-month-old WT spinal cords.

Sequencing of cat F in adult-onset NCL patients. The presence of autofluorescent lipofuscin-like storage material is characteristic of the neurodegenerative disease NCL. Comparison with the symptoms and age of onset of other mouse models of NCL suggests that cat F deficiency may represent a late-onset NCL. Consequently, to determine whether cat F is mutated in adult-onset NCL patients, sequence analysis of genomic DNA from 13 unrelated patients clinically diagnosed with late-onset NCL was performed. Exons and intron/exon boundaries of the cat F gene were sequenced and compared to published genomic sequences (GenBank accession numbers AF132894 and NT_033903). No nonsynonymous mutations were found in any of these NCL patients (not shown).

DISCUSSION

Characterization of the phenotype of mice lacking cat F revealed that cat$F^{-/-}$ mice developed progressive deficiencies in motor coordination, hind leg paraparesis, general wasting, and premature death. Histological analysis demonstrated widespread progressive accumulation of granular autofluorescence in the CNS without significant visceral involvement. EM investigation of the spinal cord confirmed the presence of membrane-bound lipofuscin granules with fingerprint profiles, a finding indicative of lysosomal lipofuscin accumulation. These findings are similar to observations in mice and humans with more gross defects in endosomal/lysosomal function (15, 21, 23, 40). However, cat F is the only endoprotease whose inactivation alone causes widespread but exclusively CNS lipofuscin accumulation.

What are the features of cat F which could account for its unexpected, nonredundant role in neuronal function? Contributing to this phenotype may be the relative lack of other potent endoproteases in normal neural tissue compared to that of the visceral organs (Fig. 3C). Certainly, very little active cat L and no cat S could be detected in spinal cord extracts, and the finding of neuronal lipofuscin accumulation in cat D-null mice (13) could also point to the limited redundancy of lysosomal endoproteases in the CNS. However, cat F is unique in that it has a long pro-region whose function is unknown. In this regard, the previously reported potent activity of cat F in lipoprotein degradation is remarkable (17, 26). Although the exact substrate of cat F in neurons is not known, we favor the view that a lipoprotein component of the lipofuscin complex is a preferential substrate of cat F. The unique, long amino-terminal pro-region of cat F may be a substrate recognition site for this putative lipoprotein. A specific function of cat F within CNS lysosomes is also suggested by the observation that both cat L/cat F and cat S/cat F double-null mice do not exhibit a more robust CNS phenotype than cat $F^{-/-}$ mice alone. This contrasts with prior reports of mice deficient in both cat B and cat L, in which cat L clearly has redundant functions in neuronal proteolysis with cat B (7). Mice with a double enzyme deficiency have a severe neuronal defect, whereas a single deficiency of either cathepsin has no CNS phenotype.

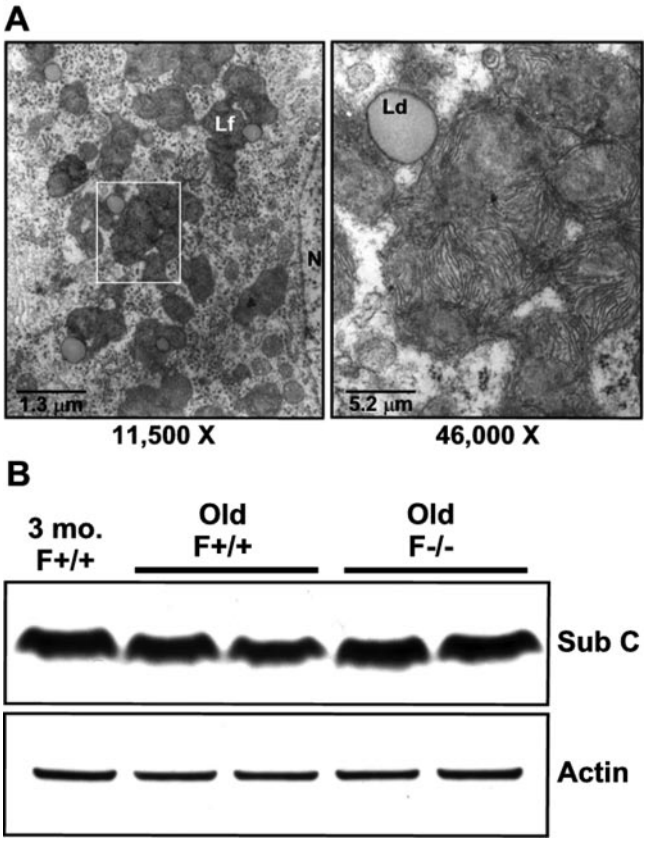

FIG. 6. Electron microscopic analysis of accumulated lipofuscin and the lack of accumulation of mitochondrial ATP synthase subunit c in old cat $F^{-/-}$ mouse spinal cord. (A) EM of cat $F^{-/-}$ lumbar spinal cord neurons. Lipofuscin (Lf) granules exhibit multilamellar mixed fingerprint profiles and frequently contain a prominent lipid droplet (Ld). N, nucleus. Left panel, ×11,500 magnification. Right panel, ×46,000 magnification of the indicated area in left panel. (B) Immunoblot of subunit c in spinal cord extracts. β-Actin was included as a loading control.

Although the precise involvement of cat F in lipofuscin accumulation is unclear, the idea that a defect in cat F, a lysosomal cysteine protease, can cause lipofuscinosis and progressive neurological defects is not unreasonable. Lysosomal storage defects frequently have neurological involvement, underscoring the critical importance of lysosomal function in the CNS (40). Most of the genes that have been identified in classic NCL and NCL-like diseases have been lysosomal or lysosome-related gene products. Proteins encoded by the NCL genes *CLN1*, *CLN2*, *CLN3*, and *CLN5* (24) and NCL-related genes *ClC-7* (15), *PPT2*, *ClC-3* (43), and cathepsin D, all localize to the lysosome. However, all of these disorders have clinical onset at a young age. Thus far, there has been little insight into the possible pathobiology of adult-onset NCL, although a few cases are caused by mild mutations of the PPT1 gene (39), and known NCL genes have been excluded by sequencing in some patients (S. E. Mole, unpublished data). The heterogeneity of clinical presentations of late-onset disease suggests that more than one gene is likely involved (9). Several naturally occurring animal models exist that appear to represent late-onset NCLs, but thus far the underlying genetic defects have also not been identified in these (5, 27, 30, 34). The present study has established another mouse model for late-onset NCL.

We considered cat F an excellent candidate for a late-onset NCL. However, sequencing of cat F in 13 late-onset NCL patients failed to identify nonsynonymous mutations in their exons and intron-exon borders. In addition, we were unable to detect in cat F-deficient mice increased accumulation of mitochondrion-derived ATP synthase subunit c, the most prominent lipofuscin component of most human NCLs (Fig. 6B). Whether cat F deficiency leads to a phenocopy of the known NCLs and reveals a novel lipofuscin capable of causing progressing neuronal dysfunction in humans remains to be defined. Our findings may be relevant as well to other complex neurodegenerative processes in which lipofuscin accumulates (36). A number of unexplained adult onset peripheral neuropathies are linked to the region from 11q12 to 11q14 region containing the cat F gene (18, 42). However, some of these have recently been shown to be caused by mutations in BSCL2 and are inherited in an autosomal dominant manner (12). The demonstration that murine cat F deficiency leads to progressive neuronal dysfunction makes the cat F gene still an excellent candidate site for mutations leading to some forms of late-onset NCL, and it is to be hoped that these cases will increasingly come to the attention of research laboratories allowing the underlying genes to be identified.

ACKNOWLEDGMENTS

This study was supported by grants from the National Institutes of Health, HL48261 (H.A.C.), the Sandler Foundation, the Wellcome Trust UK (054606; S.E.M.), and the Batten Disease Support and Research Association.

We thank the families and their physicians for contributing to this study. We thank Guo-Ping Shi for his help with the initial studies of cathepsin F genomic clones, Amos Baruch (Celera Diagnostics) for cat F polyclonal antibodies, Peter T. Ohara (UCSF) for his surgical expertise, and members of Henry J. Ralston III's laboratory (UCSF) for assistance with EM.

REFERENCES

1. **Berkovic, S. F., F. Andermann, E. Andermann, S. Carpenter, and L. Wolfe.** 1988. Kufs disease: clinical features and forms. Am. J. Med. Genet. **5**(Suppl.)**:**105–109.
2. **Brunk, U. T., and A. Terman.** 2002. Lipofuscin: mechanisms of age-related accumulation and influence on cell function. Free Radic. Biol. Med. **33:**611–619.
3. **Chapman, H. A., R. J. Riese, and G. P. Shi.** 1997. Emerging roles for cysteine proteases in human biology. Annu. Rev. Physiol. **59:**63–88.
4. **Deussing, J., K. Tisljar, A. Papazoglou, and C. Peters.** 2000. Mouse cathepsin F: cDNA cloning, genomic organization and chromosomal assignment of the gene. Gene **251:**165–173.
5. **Drogemuller, C., A. Wohlke, and O. Distl.** 2005. Evaluation of the canine TPP1 gene as a candidate for neuronal ceroid lipofuscinosis in Tibetan Terrier and Polish Owczarek Nizinny dogs. Anim. Genet. **36:**178–179.
6. **Elleder, M., J. Sokolova, and M. Hrebicek.** 1997. Follow-up study of subunit c of mitochondrial ATP synthase (SCMAS) in Batten disease and in unrelated lysosomal disorders. Acta Neuropathol. **93:**379–390.
7. **Felbor, U., B. Kessler, W. Mothes, H. H. Goebel, H. L. Ploegh, R. T. Bronson, and B. R. Olsen.** 2002. Neuronal loss and brain atrophy in mice lacking cathepsins B and L. Proc. Natl. Acad. Sci. USA **99:**7883–7888.
8. **Goebel, H. H., S. E. Mole, and B. D. Lake.** 1999. The neuronal ceroid lipofuscinoses (Batten disease), p. 211. IOS Press, Amsterdam, The Netherlands.
9. **Goebel, H. H., S. S. Schochet, M. Jaynes, W. Bruck, A. Kohlschutter, and F. Hentati.** 1999. Progress in neuropathology of the neuronal ceroid lipofuscinoses. Mol. Genet. Metab. **66:**367–372.
10. **Gupta, P., A. A. Soyombo, A. Atashband, K. E. Wisniewski, J. M. Shelton, J. A. Richardson, R. E. Hammer, and S. L. Hofmann.** 2001. Disruption of PPT1 or PPT2 causes neuronal ceroid lipofuscinosis in knockout mice. Proc. Natl. Acad. Sci. USA **98:**13566–13571.
11. **Gupta, P., A. A. Soyombo, J. M. Shelton, I. G. Wilkofsky, K. E. Wisniewski,**

J. A. Richardson, and S. L. Hofmann. 2003. Disruption of PPT2 in mice causes an unusual lysosomal storage disorder with neurovisceral features. Proc. Natl. Acad. Sci. USA **100:**12325–12330.
12. **Irobi, J., P. Van den Bergh, L. Merlini, C. Verellen, L. Van Maldergem, I. Dierick, N. Verpoorten, A. Jordanova, C. Windpassinger, E. De Vriendt, V. Van Gerwen, M. Auer-Grumbach, K. Wagner, V. Timmerman, and P. De Jonghe.** 2004. The phenotype of motor neuropathies associated with BSCL2 mutations is broader than Silver syndrome and distal HMN type V. Brain **127:**2124–2130.
13. **Ivanov, S. V., J. M. Ward, L. Tessarollo, D. McAreavey, V. Sachdev, L. Fananapazir, M. K. Banks, N. Morris, D. Djurickovic, D. E. Devor-Henneman, M. H. Wei, G. W. Alvord, B. Gao, J. A. Richardson, J. D. Minna, M. A. Rogawski, and M. I. Lerman.** 2004. Cerebellar ataxia, seizures, premature death, and cardiac abnormalities in mice with targeted disruption of the *Cacna2d2* gene. Am. J. Pathol. **165:**1007–1018.
14. **Jasmin, L., G. Janni, T. M. Moallem, D. A. Lappi, and P. T. Ohara.** 2000. Schwann cells are removed from the spinal cord after effecting recovery from paraplegia. J. Neurosci. **20:**9215–9223.
15. **Kasper, D., R. Planells-Cases, J. C. Fuhrmann, O. Scheel, O. Zeitz, K. Ruether, A. Schmitt, M. Poet, R. Steinfeld, M. Schweizer, U. Kornak, and T. J. Jentsch.** 2005. Loss of the chloride channel ClC-7 leads to lysosomal storage disease and neurodegeneration. EMBO J. **24:**1079–1091.
16. **Koike, M., H. Nakanishi, P. Saftig, J. Ezaki, K. Isahara, Y. Ohsawa, W. Schulz-Schaeffer, T. Watanabe, S. Waguri, S. Kametaka, M. Shibata, K. Yamamoto, E. Kominami, C. Peters, K. von Figura, and Y. Uchiyama.** 2000. Cathepsin D deficiency induces lysosomal storage with ceroid lipofuscin in mouse CNS neurons. J. Neurosci. **20:**6898–6906.
17. **Lindstedt, L., M. Lee, K. Oorni, D. Bromme, and P. T. Kovanen.** 2003. Cathepsins F and S block HDL3-induced cholesterol efflux from macrophage foam cells. Biochem. Biophys. Res. Commun. **312:**1019–1024.
18. **Macedo-Souza, L. I., F. Kok, S. Santos, S. C. Amorim, A. Starling, A. Nishimura, K. Lezirovitz, A. M. Lino, and M. Zatz.** 2005. Spastic paraplegia, optic atrophy, and neuropathy is linked to chromosome 11q13. Ann. Neurol. **57:**730–737.
19. **Malgaroli, A., and R. W. Tsien.** 1992. Glutamate-induced long-term potentiation of the frequency of miniature synaptic currents in cultured hippocampal neurons. Nature **357:**134–139.
20. **Meara, J. P., and D. H. Rich.** 1996. Mechanistic studies on the inactivation of papain by epoxysuccinyl inhibitors. J. Med. Chem. **39:**3357–3366.
21. **Mitchison, H. M., M. J. Lim, and J. D. Cooper.** 2004. Selectivity and types of cell death in the neuronal ceroid lipofuscinoses. Brain Pathol. **14:**86–96.
22. **Mitchison, H. M., and S. E. Mole.** 2001. Neurodegenerative disease: the neuronal ceroid lipofuscinoses (Batten disease). Curr. Opin. Neurol. **14:**795–803.
23. **Mole, S.** 2004. Neuronal ceroid lipofuscinoses (NCL). Eur. J. Paediatr Neurol. **8:**101–103.
24. **Mole, S. E.** 2004. The genetic spectrum of human neuronal ceroid-lipofuscinoses. Brain Pathol. **14:**70–76.
25. **Mole, S. E.** 1996. Recent advances in the molecular genetics of the neuronal ceroid lipofuscinoses. J. Inherit. Metab. Dis. **19:**269–274.
26. **Oorni, K., M. Sneck, D. Bromme, M. O. Pentikainen, K. A. Lindstedt, M. Mayranpaa, H. Aitio, and P. T. Kovanen.** 2004. Cysteine protease cathepsin F is expressed in human atherosclerotic lesions, is secreted by cultured macrophages, and modifies low density lipoprotein particles in vitro. J. Biol. Chem. **279:**34776–34784.
27. **Palmer, D. N., R. D. Jolly, H. C. van Mil, J. Tyynela, and V. J. Westlake.** 1997. Different patterns of hydrophobic protein storage in different forms of neuronal ceroid lipofuscinosis (NCL, Batten disease). Neuropediatrics **28:**45–48.
28. **Palmer, J. T., D. Rasnick, J. L. Klaus, and D. Bromme.** 1995. Vinyl sulfones as mechanism-based cysteine protease inhibitors. J. Med. Chem. **38:**3193–3196.
29. **Rawlings, N. D., and A. J. Barrett.** 1999. Tripeptidyl-peptidase I is apparently the CLN2 protein absent in classical late-infantile neuronal ceroid lipofuscinosis. Biochim. Biophys. Acta **1429:**496–500.
30. **Rossmeisl, J. H., Jr., R. Duncan, J. Fox, E. S. Herring, and K. D. Inzana.** 2003. Neuronal ceroid-lipofuscinosis in a Labrador retriever. J. Vet. Diagn. Investig. **15:**457–460.
31. **Santamaria, I., G. Velasco, A. M. Pendas, A. Paz, and C. Lopez-Otin.** 1999. Molecular cloning and structural and functional characterization of human cathepsin F, a new cysteine proteinase of the papain family with a long propeptide domain. J. Biol. Chem. **274:**13800–13809.
32. **Selak, S., and M. J. Fritzler.** 2004. Altered neurological function in mice immunized with early endosome antigen 1. BMC Neurosci. **5:**2.
33. **Shi, G. P., R. A. Bryant, R. Riese, S. Verhelst, C. Driessen, Z. Li, D. Bromme, H. L. Ploegh, and H. A. Chapman.** 2000. Role for cathepsin F in invariant chain processing and major histocompatibility complex class II peptide loading by macrophages. J. Exp. Med. **191:**1177–1186.
34. **Siso, S., C. Navarro, D. Hanzlicek, and M. Vandevelde.** 2004. Adult onset thalamocerebellar degeneration in dogs associated to neuronal storage of ceroid lipopigment. Acta Neuropathol. **108:**386–392.
35. **Tang, C. H., and E. A. Grimm.** 2004. Depletion of endogenous nitric oxide enhances cisplatin-induced apoptosis in a p53-dependent manner in melanoma cell lines. J. Biol. Chem. **279:**288–298.
36. **Terman, A., and U. T. Brunk.** 2004. Lipofuscin. Int. J. Biochem. Cell. Biol. **36:**1400–1404.
37. **Turk, B., V. Turk, and D. Turk.** 1997. Structural and functional aspects of papain-like cysteine proteinases and their protein inhibitors. Biol. Chem. **378:**141–150.
38. **Tyynela, J., J. D. Cooper, M. N. Khan, S. J. Shemilts, and M. Haltia.** 2004. Hippocampal pathology in the human neuronal ceroid-lipofuscinoses: distinct patterns of storage deposition, neurodegeneration, and glial activation. Brain Pathol. **14:**349–357.
39. **van Diggelen, O. P., S. Thobois, C. Tilikete, M. T. Zabot, J. L. Keulemans, P. A. van Bunderen, P. E. Taschner, M. Losekoot, and Y. V. Voznyi.** 2001. Adult neuronal ceroid lipofuscinosis with palmitoyl-protein thioesterase deficiency: first adult-onset patients of a childhood disease. Ann. Neurol. **50:**269–272.
40. **Vellodi, A.** 2005. Lysosomal storage disorders. Br. J. Haematol. **128:**413–431.
41. **Wang, B., G. P. Shi, P. M. Yao, Z. Li, H. A. Chapman, and D. Bromme.** 1998. Human cathepsin F. Molecular cloning, functional expression, tissue localization, and enzymatic characterization. J. Biol. Chem. **273:**32000–32008.
42. **Windpassinger, C., K. Wagner, E. Petek, R. Fischer, and M. Auer-Grumbach.** 2003. Refinement of the Silver syndrome locus on chromosome 11q12-q14 in four families and exclusion of eight candidate genes. Hum. Genet. **114:**99–109.
43. **Yoshikawa, M., S. Uchida, J. Ezaki, T. Rai, A. Hayama, K. Kobayashi, Y. Kida, M. Noda, M. Koike, Y. Uchiyama, F. Marumo, E. Kominami, and S. Sasaki.** 2002. CLC-3 deficiency leads to phenotypes similar to human neuronal ceroid lipofuscinosis. Genes Cells **7:**597–605.